

LARGE-EDDY AND DIRECT SIMULATIONS OF SINK FLOWS OVER ROUGH WALLS

Junlin Yuan and Ugo Piomelli

Department of Mechanical and Materials Engineering
Queen's University
Kingston (Ontario), Canada
junlin.yuan@queensu.ca, ugo@appsci.queensu.ca

ABSTRACT

Turbulent sink-flow boundary layers over smooth and rough walls are studied using large-eddy and direct numerical simulations. Various acceleration levels are applied, yielding a wide range of Reynolds number ($Re_\theta = 372 - 2748$). The effects of acceleration and roughness on the flow are investigated. The results highlight that acceleration and roughness have opposite effects, consistent with previous investigations. Acceleration is found more important than roughness on outer-region turbulence. In the near wall, roughness causes spatial variations of the mean velocity that are correlated with the geometry. The streaky structure of the near-wall layer is significantly modified.

INTRODUCTION

Turbulent boundary layers subject to a favorable pressure gradients (FPG) are found in many engineering applications, including airfoils, turbine blades or curved duct. The acceleration can be characterized by the parameter $K = (v/U_\infty^2)(dU_\infty/dx)$ (U_∞ is the freestream velocity). When the acceleration is sufficiently large, the flow may revert to a laminar or quasi-laminar state. The accelerating boundary layer that lends itself most to analysis and simulation (although difficult to achieve experimentally) is the flow in a two-dimensional convergent duct, known as sink flow, for which a laminar solution exists and similarity analysis can be applied in turbulent flow. The turbulent sink flow has been studied numerically (Spalart, 1986; Esmaili & Piomelli, 1993) and experimentally (Jones & Launder, 1972; Chambers *et al.*, 1983; Jones *et al.*, 2001; McEligot & Eckelmann, 2006; Dixit & Ramesh, 2008, 2010); in this type of flows, K and the Reynolds number remain constant, resulting in statistical similarity in the flow direction. Therefore, a sink flow is substantially less expensive computationally, compared to spatially developing accelerating flows. In smooth-wall sink flows, the acceleration results in thickening of the viscous sublayer, damping of fluctuations especially in the vertical component, lower bursting rate, and larger near-wall coherent structures. Spalart (1986) showed that turbulence cannot be sustained if $K > K_{crit} \simeq 3 \times 10^{-6}$.

In realistic spatially developing boundary layers, of course, the acceleration cannot act for infinite distances, and complete relaminarization occurs rarely. However, the state of the flow is still significantly altered by strong acceleration, and even the mean velocity profile is modified.

Reviews of existing knowledge can be found in sev-

eral landmark articles (Narasimha & Sreenivasan, 1973; Narasimha, 1985; Narasimha & Sreenivasan, 1979). Here we summarize the major points only. Experimental investigations of relaminarization due to flow acceleration started in the early 1960s. Among the major findings of these studies was the fact that, at least in the outer region of the boundary layer, dissipation remains smaller than production. Narasimha & Sreenivasan (1973) conjectured that, since the streamwise and wall-normal fluctuations do not lose their correlation, relaminarization is due to pressure forces dominating over nearly frozen Reynolds stresses. Recent simulations of accelerating flows over smooth, flat plates Piomelli *et al.* (2000); De Prisco *et al.* (2007) show that, in the region of maximum acceleration, frozen turbulence advected from upstream is still present, but it does not adjust to the freestream acceleration.

Roughness plays an important role in many fields of study. Systematic experimental studies of turbulent flow in rough pipes were carried out by Nikuradse (1933) and Colebrook (1939). Since then, a substantial amount of work has been done to understand the dynamics of turbulent flows over rough-walls, both for engineering and atmospheric applications. Reviews by Raupach and co-workers (Raupach & Thom, 1981; Raupach *et al.*, 1991) and Finnigan (2000) summarize the research on roughness in atmospheric applications, while those by Raupach *et al.* (1991) and Jiménez (2004) discuss engineering flows.

Investigations of the interaction between roughness and pressure gradients have been carried out only recently. Tachie *et al.* (2007) studied open channel flows with bar roughness; the FPG resulted from converging side-walls. From the study of a wide range of k_s^+ they concluded that, while in the hydraulically smooth regime the flow responses were similar to those on a smooth wall, in the cases of fully rough flows no apparent FPG effect was observed on drag characteristics, the mean flow, and turbulent quantities. It is worth noting that the streamwise domain under study might be too limited for full FPG effects to take place, and that the accelerating flows were strongly non-equilibrium.

Cal *et al.* (2008, 2009) studied quasi-equilibrium boundary-layer flows on a tilted plane with sand-grain roughness and mild acceleration; the acceleration was applied for a considerable distance for both the fully rough and transitionally rough flows. They observed a general increase of friction coefficient C_f and decrease of Reynolds number based on momentum thickness, Re_θ , as acceleration was imposed on the rough wall. Competing effects

August 28 - 30, 2013 Poitiers, France

of K and roughness were found on the mean flow, and in the outer layer of the Reynolds stresses; however, instead of damping fluctuations (as in the outer layer), acceleration significantly intensified them close to the rough wall, an effect opposite to a smooth-wall flow. Again it is not clear whether these effects were limited to the early stage of acceleration, or whether they were due to the mild levels of acceleration.

To answer some of the questions raised by recent experimental studies (in particular, to eliminate the effects of spatial variation of the acceleration) in this paper we carry out a parametric study of acceleration parameter K and roughness in the transitionally rough regime for a turbulent sink-flow boundary layer. In the following, first we present the model used, including the numerical scheme, the turbulence parameterization and the modelling of the roughness. We will then discuss the simulation results, stressing the effects of k , k^+ and K . A summary of the conclusions will end the paper.

PROBLEM FORMULATION

The motion of an incompressible flow of a newtonian fluid is governed by the equations of conservation of mass and momentum:

$$\frac{\partial u_i}{\partial x_i} = 0, \quad (1)$$

$$\frac{\partial u_j}{\partial t} + \frac{\partial u_i u_j}{\partial x_i} = -\frac{\partial P}{\partial x_j} + \frac{1}{Re} \nabla^2 u_j. \quad (2)$$

The equations have been made dimensionless using a reference velocity and length, U_∞ and X (which will be specified later). x_1 , x_2 and x_3 (or x , y and z) are, respectively, the streamwise, wall-normal and spanwise directions, and u_i (or u , v and w) are the velocity components in those directions; $P = p/\rho$ is the modified pressure, ρ the density and $Re = U_\infty X/\nu$ the Reynolds number. In LES, Equations (1-2) are solved for filtered quantities, and the divergence of the sub-grid stress tensor, $\tau_{ij} = \overline{u_i u_j} - \overline{u_i} \overline{u_j}$, appears on the right hand side of the momentum equation. In the present study, τ_{ij} is modeled using the Lagrangian-Averaged Eddy-Viscosity model (Meneveau *et al.*, 1996).

To calculate the sink flow we use the approach proposed by Spalart (1986): the domain is transformed into similarity coordinates (x, η, z) , with $\eta = yX_o/X$. Here, X_o is a constant and X the distance from the sink. If the boundary-layer thickness δ is much smaller than X , since the turbulent fluctuations vary on a length scale $o(\delta) \ll X$, we can consider a domain centered around a position X_o , assume that the turbulence is spatially homogeneous, and include the effect of the acceleration through growth terms that can be obtained from the transformation of the equations into the similarity coordinates, followed by a multiple-scale procedure to simplify the equations. The effect of the acceleration appears through growth terms G_u and G_w , which are added to the right-hand-side of u - and w -momentum equations:

$$G_u = -\frac{\langle u \rangle}{X_o} (\langle u \rangle + 2u') + \frac{U_\infty^2}{X_o}, \quad G_w = -\frac{\langle u \rangle}{X_o} w', \quad (3)$$

where $\langle \cdot \rangle$ denotes an appropriate average, and u' and w' are fluctuations from the averages. With this transformation,

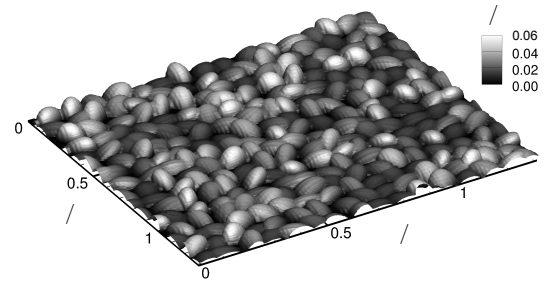


Figure 1. Visualization of sand-grain roughness $R3$ for $1/8$ of the domain.

only two parameters are present: the acceleration parameter K (which is also an inverse Reynolds number: $K = \nu/U_\infty X$) and the roughness height, $\bar{k} = k/X_o$, where $k = k_s$ for the sand-grain roughness used in this study. In the following, for simplicity, η is replaced with y .

The simulations are performed using a well-validated code that solves the governing equations (1-2) on a staggered grid using second-order, central differences for all terms, a second-order accurate semi-implicit time advancement, and MPI parallelization (Keating *et al.*, 2004). Periodic boundary conditions are used in the streamwise and spanwise directions (since the flow is assumed to be homogeneous on the scale $\delta \ll X$). A free-slip boundary condition is imposed on the top boundary.

An immersed-boundary method is used to represent the rough surfaces. We use the roughness model proposed by Scotti (2006): a virtual sand-paper is constructed from randomly oriented and distributed ellipsoids of the same shape and size (with the three semi-axes equaling k , $1.5k$, and $2k$); this model was found to give $k_s \approx k$ in the transitionally rough regime. The volume fraction of each cell occupied by the fluid (volume of fluid, or VOF) is calculated in pre-processing, and the force (F_i in the x_i direction) exerted by the roughness to the flow is imposed on the right-hand side of the momentum equation to reduce the velocity by an amount proportional to the solid volume in each cell. The streamwise component of the force used to drive the velocity to zero within the immersed boundary can be integrated to yield the drag force, $f_d(x, z)$. Note that f_d includes both the pressure and viscous drags. A typical surface is shown in Figure 1.

A total of 12 simulations were run, identified by $KnRm$, where $n = 1, \dots, 4$ denotes varying acceleration parameters K , and $m = 0, \dots, 3$ different roughness heights. Table 1 gives the values of K , \bar{k} , and k^+ in all cases. k^+ values within a 25% range are considered constant; thus, we will consider cases K2R1, K3R2 and K4R3 as having approximately the same value of k^+ . In all cases, $\delta/k \geq 25$, and k^+ is in the transitionally rough regime; Re_θ ranges between 372 and 2853.

Due to the wide variation of the Reynolds number, LES are used for the cases with milder accelerations (K1 and K2), while direct simulations are used for cases K3 and K4. The domain size in all cases is $0.2X_o \times 0.06X_o \times 0.04X_o$, equivalent to approximately $9\delta \times 3\delta \times 2\delta$. The domain sizes in x and z directions are similar to those used by Spalart (1986), and the streamwise and spanwise two-point correlations of the turbulent fluctuations, calculated at $y = 0.5\delta$, fall below 0.1 at half the domain length or width. 768 grid points were used in x and 512 in z for cases K1, K2 and K3. For the K4 cases, 384 and 256 points only were

Table 1. Values of roughness Reynolds number k^+ and simulation parameters.

	K1	K2	K3	K4	
K	0.45×10^{-6}	0.80×10^{-6}	1.50×10^{-6}	2.50×10^{-6}	
R0 (smooth)	0	0	0	0	their contri
R1 ($\bar{k} = 3.0 \times 10^{-4}$)	36.3	20.2	10.6	–	
R2 ($\bar{k} = 6.0 \times 10^{-4}$)	–	45.9	23.4	13.4	
R3 ($\bar{k} = 9.5 \times 10^{-4}$)	–	–	41.6	23.8	

used in x and z . The number of points in the wall-normal direction above the roughness elements was around 220 for all cases; simulations with larger \bar{k} required more points to resolve the roughness elements.

Uniform grids are used in x and z directions, while stretching is applied in the y direction outside of the roughness layer. In DNS, Δx^+ and Δz^+ are less than 10 and 3, respectively, and the minimum $\Delta y^+ < 0.5$ in the region below the top of the roughness elements ($y < 1.5k$). In LES $\Delta x^+ = 17 - 30$, $\Delta z^+ = 6 - 9$, and the $\Delta y^+ < 1$ in the region $y < 1.5k$. The stretching rate of the y grid is kept below 4% in all cases. Note that even the LES is highly resolved, with grid sizes only marginally worse than those of direct simulations in the literature. Between 20 to 100 million total grid points were required. The roughness geometry is resolved by no less than 16 grid points in the (x, z) plane, and by more than 30 grid points in the y direction.

In the following, the angle brackets $\langle \cdot \rangle$ denote quantities that are averaged in time and over the homogeneous directions x and z . $U_i(y)$ is the time- and space-averaged velocity whereas $\langle \cdot \rangle_{xz}$ and $\langle \cdot \rangle_t$ denote only averaging over the homogeneous direction or in time: $U_i = \langle u_i \rangle$; $\tilde{U}_i(x, y, z) = \langle u_i \rangle_t - U_i$ is the deviation of the local time-averaged velocity from the time- and space-averaged one. The turbulent fluctuation u'_i are calculated by subtracting the time-averaged velocity from the total one:

$$u'_i = u_i - \langle u_i \rangle_t = u_i - (U_i + \tilde{U}_i). \quad (4)$$

Averages are computed over $T \simeq 30\delta/u_\tau$ units after the transient, a sample size sufficient to obtain converged statistics.

RESULTS

Flow statistics

The Reynolds number based on momentum thickness θ , $Re_\theta = \theta U_\infty/\nu$, and the skin-friction coefficient, $C_f = 2\tau_w/\rho U_\infty^2$ (where τ_w is the wall stress) are shown in Figure 2. Good agreement is obtained with available experimental (Jones & Launder, 1972; Dixit & Ramesh, 2010) and numerical (Spalart, 1986) data for smooth walls. Re_θ decreases with increasing K and increases with roughness height, a phenomenon also observed by Cal *et al.* (2008). C_f increases with K in the study by Cal *et al.* (2008), while results obtained by Tachie *et al.* (2007) showed negligible variation of C_f with K . In the current study an increase of K while \bar{k} is constant is found to decrease C_f . Roughness increases C_f , a result observed in all studies. However, $u_\tau/U_\infty = (C_f/2)^{1/2}$ is only mildly affected by K and

\bar{k} . Therefore, the viscous length-scale

$$\bar{\delta}_v \equiv (\nu/u_\tau)/X_o = K(U_\infty/u_\tau) \quad (5)$$

is almost linearly proportional to K , and $k^+ = \bar{k}/\bar{\delta}_v \sim \bar{k}/K$, can be viewed as a relative measure of the effects of roughness and acceleration. Figures 2(b) and (d) show that Re_θ is more affected by the acceleration effect, and C_f by the roughness.

Figure 3 shows the mean velocity profile in wall units for calculations with increasing acceleration (Figure 3(a)) and roughness height (Figure 3(b)). In most cases (the main exception being the high-acceleration, low-roughness one, K4R2), we observe a logarithmic layer, which acceleration displaces upwards and roughness downwards. Non-universal log-law constants have been used to describe equilibrium sink flows with similar or lower levels of acceleration compared to the current study (Dixit & Ramesh, 2008, 2010), but in our calculations the von Kármán constant κ (calculated by considering the plateau region of $y^+ dU^+/dy^+$) was found to be within the accepted range ($\kappa \simeq 0.4$) except in case K4R2. In this case, $k^+ \simeq 10$, close to the hydraulically smooth regime, and the pressure gradient is strong, leading to a case close to reverse transition. On the smooth wall, Dixit & Ramesh (2008) observed an 18% increase of κ as K increased from 7.71×10^{-7} to 2.9×10^{-6} ; in the present calculation for the rough wall R2, a sudden increase of κ as K approaches K4 indicates that flow reversion occurs only when the flow is nearly in the hydraulically smooth regime; at this point, κ takes the smooth-wall value. For higher roughness heights k^+ , κ is insensitive to the strengthening of acceleration.

Since the slope of the logarithmic region is close to the universal value, the velocity deficit could be quantified using a generalized roughness function, ΔU^+ (Figure 4). We observe that the sink-flow results collapse with those from experimental studies on equilibrium pipe flows. The roughness-induced momentum deficit is not strongly affected by either acceleration or roughness; instead, it is affected by the ratio between the strengths of the two, measured by k^+ . In non-equilibrium accelerating boundary layers, Tachie *et al.* (2007) found, based on the assumption of a universal log-law, that ΔU^+ is affected by roughness height but not by acceleration. This does not necessarily contradict the current results, since, in their study, k^+ is not significantly affected by K either. The current work serves to clarify that both K and \bar{k} play a role in determining the mean velocity deficit in sink flows.

The Reynolds stresses are presented in Figure 5. For low blockage-ratio (k/δ), roughness does not affect the Reynolds stresses (normalized by u_τ^2) in the outer layer of a high-Reynolds-number ZPG boundary layer. Here, it is

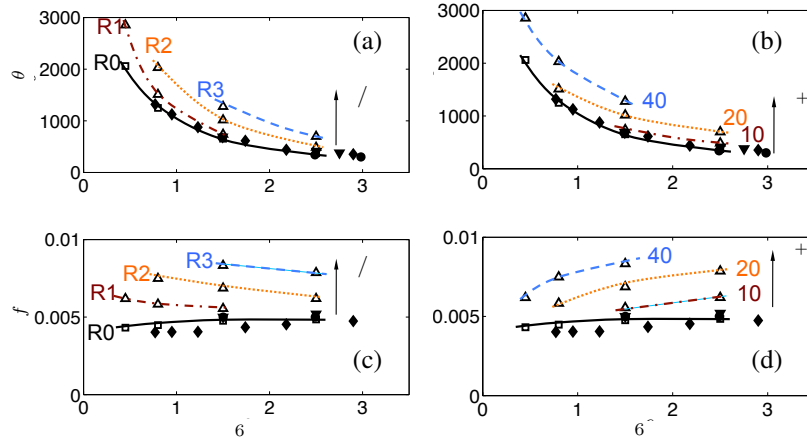


Figure 2. Effects of roughness and acceleration on (a), (b) the Reynolds number and (c), (d) the friction coefficient. Lines connect cases with constant k/δ in (a) and (c), and connect cases with constant k^+ in (b) and (d). Hollow symbols are data from current study: \square smooth; \triangle rough. Solid symbols are reference data: \blacklozenge Dixit & Ramesh (2010); \bullet Jones & Launder (1972); \blacktriangledown Spalart (1986).

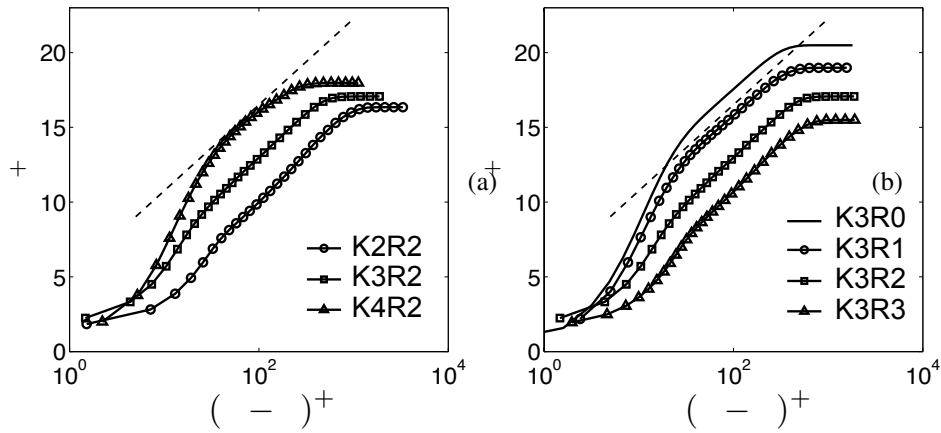


Figure 3. Mean velocity profiles in inner scaling. (a) Effect of K ; (b) Effect of \bar{k} . --- Universal logarithmic law.

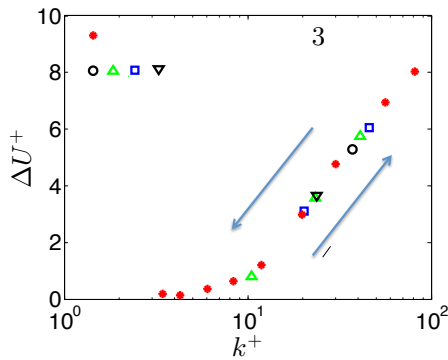


Figure 4. Dependence of roughness function ΔU^+ (case K4R2 not shown) on k^+ .

found that wall similarity applies to boundary layers subjected to mild acceleration (in which the Reynolds number is not significantly reduced), such as the K2 cases (Fig 5(b)) (with $Re_\theta = 1248 - 2028$ and $k/\delta \lesssim 0.03$). On the other hand, in the K4 cases (Fig 5(a)) the streamwise and wall-normal Reynolds stresses do not collapse. Specifically, the increase of $\langle u'u' \rangle$ due to roughness is less fast than the in-

crease of u_τ^2 , while the increase of $\langle v'v' \rangle$ is faster than that of u_τ^2 . In these cases, k/δ are similar to those in the K2 cases, but the Reynolds numbers are much lower ($Re_\theta = 372 - 696$). Case K4R0 and K4R2 are in the reverse-transitional state; the wall similarity hypothesis, based on fully turbulent flows, is not expected to hold under such conditions.

From here on, focus is placed on the cases away from the reverse-transitional state, which appear more commonly in realistic FPG boundary layers. In Figure 6, the Reynolds stresses are compared for three cases: Cases K1R1 and K3R1 show the effects of K increase only, while cases K3R1 and K3R3 show the effects of \bar{k} increase only. K1R1 and K3R3 have $k^+ \approx 40$ while K3R1 corresponds to a lower $k^+ \approx 10$. Similar to the effects on smooth-wall flows, an increase of K increases $\langle u'u' \rangle$ in the near-wall region, in qualitative agreement with the transitionally-rough-flow observation by Cal *et al.* (2008). In that study, however, $\langle v'v' \rangle$ increased with acceleration for $y \lesssim 0.4\delta_{95}$ and did not noticeably vary farther away from the wall; similar near-wall intensification of $\langle v'v' \rangle$ was also observed in non-equilibrium FPG boundary layers (Yuan, 2011). The current results, however, show a clear $\langle v'v' \rangle$ decrease throughout the boundary layer. This difference might indicate that, compared to $\langle u'u' \rangle$, $\langle v'v' \rangle$ is more sensitive to the stage of flow develop-

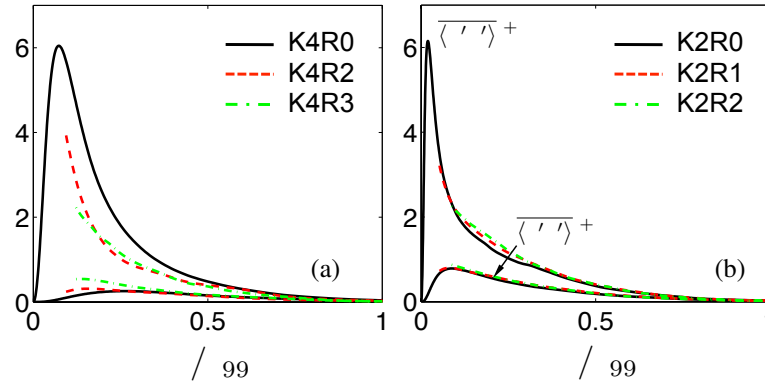


Figure 5. Roughness effects on the streamwise and vertical normal components of the Reynolds stress tensor, normalized by u_τ , in cases with (a) K4 and (b) K2. Only the outer parts ($y > 3k$) of the rough-wall profiles are shown.

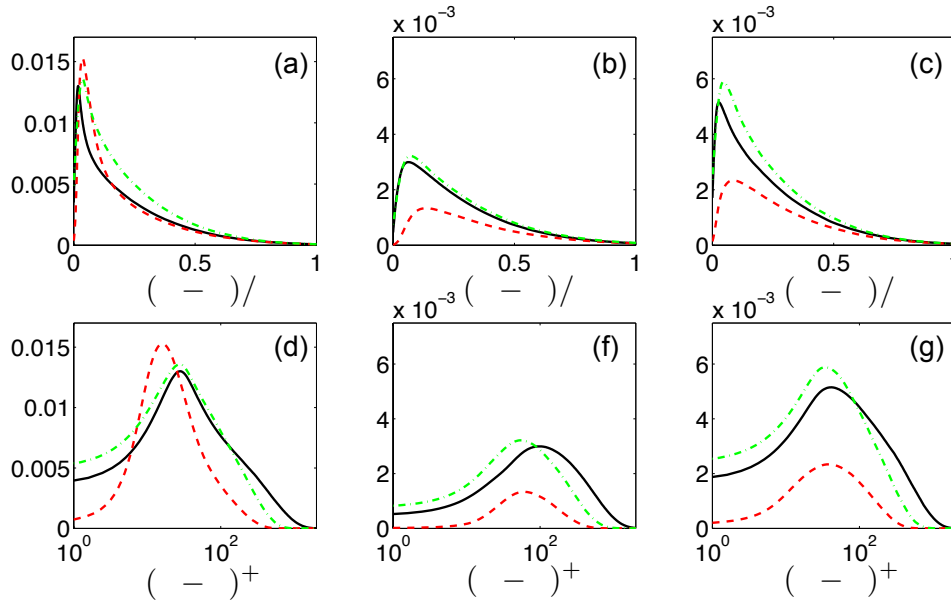


Figure 6. Effects of K and \bar{k} on (a,d) the streamwise, (b,f) vertical, and (c,g) spanwise normal Reynolds stresses, demonstrated by cases K1R1 (—), K3R1 (---), and K3R3 (-·-·-). Both inner scaling (a-c) and outer scaling (d-g) are used. The Reynolds stresses are normalized by U_∞^2 .

ment in an accelerating flow over roughness. On the other hand, the roughness height clearly increases both Reynolds stress components throughout the boundary layer, a result supported by Cal *et al.* (2008). The effects of K and \bar{k} are similar in magnitude in the outer layer ($y \geq 3k$), while in the wall region ($(y-d)^+ \leq 60$),¹ similarity exists for Reynolds stress profiles in cases with the same k^+ .

The Reynolds stress anisotropy tensor b_{ij} is defined as

$$b_{ij} = \frac{\langle u_i u_j \rangle}{\langle u_k u_k \rangle} - \frac{\delta_{ij}}{3}. \quad (6)$$

In one-dimensional turbulence, the relevant component of the normal anisotropy components, $b_{\alpha\alpha}$ (no summation on Greek indices), is $2/3$, while the other normal components are equal to $-1/3$. Anisotropies for the same three rough

cases are shown in Figure 7. It can be seen that the outer-layer anisotropy is determined by K , consistent with the wall similarity valid for these cases. In the wall region, on the other hand the anisotropy shows a k^+ -based similarity similar to that for the Reynolds stresses shown in Figure 6.

Turbulence structure

In the current rough and smooth cases, sweep (Quadrant 2 – Q2) and ejection (Quadrant 4 – Q4) events each contribute between 75% and 88% of the total Reynolds shear stress. The vertical distributions of the quadrant contributions are compared in Figure 8 for smooth and rough cases. The smooth-wall profiles resemble those in non-accelerating flows (Kim *et al.*, 1987): sweeps and ejections are more significant in the outer and near-wall regions, respectively; their contributions are equal at $y^+ \approx 10 - 15$. The main effect of K is to increase the Q2 contribution and to decrease that of Q4 for $(y-d)^+ > 20$. Less difference in the near-wall region is observed. In rough-wall sink flows, near the wall, Q2 contributions from the rough cases are 30% higher than on a smooth wall. A compar-

¹The zero-plane displacement d , is defined as the vertical location where the drag of the roughness element appears to act (*i.e.*, the centroid of the local drag profile). With the current sand-grain model, $d/k \approx 0.8$, insensitive to the value of K .

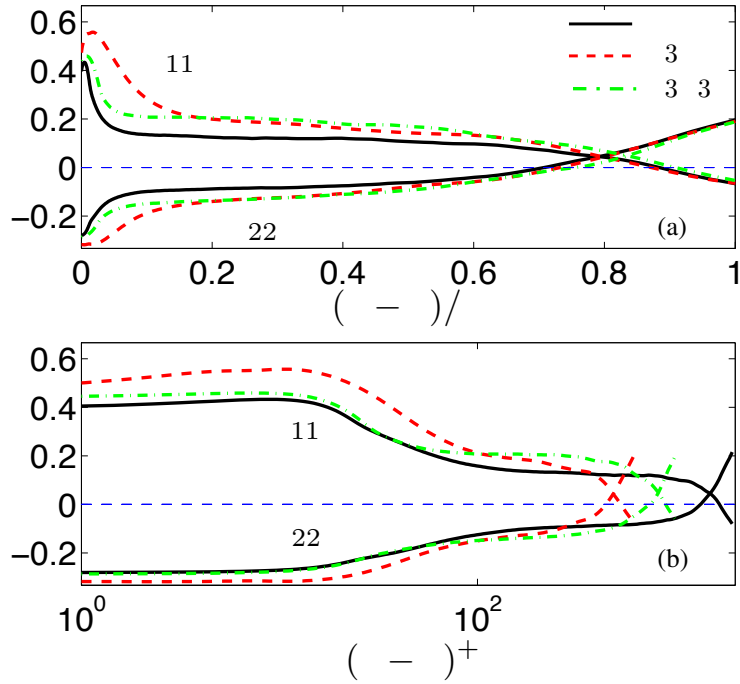


Figure 7. Streamwise and wall-normal components of the anisotropy tensor for rough cases K1R1, K3R1, and K3R3 plotted in (a) inner and (b) outer scaling.

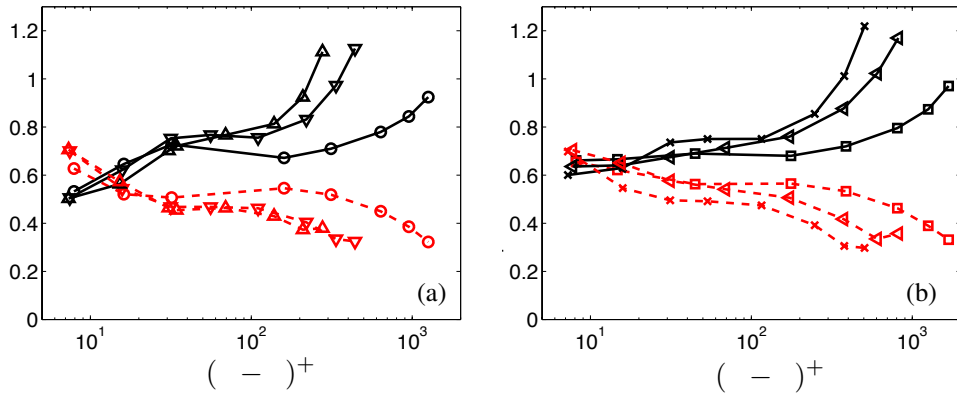


Figure 8. Quadrant contributions from Q2 (—) and Q4 (---) events. (a) Smooth wall: \circ K1R0, ∇ K3R0, \triangle K4R0; (b) rough wall: \square K1R1, \times K3R1, \triangleleft K3R3. Vertical locations vary from $(y-d)^+ = 15$ to $(y-d)/\delta = 0.4$.

ison of cases K3R1 and K3R3 show that an increase of \bar{k} tends to restore the profiles towards the K1R1 case by decreasing Q2 and promoting Q4 contributions in the region $15 \lesssim (y-d)^+ \lesssim 50$. The role of roughness in intensifying ejections close to the wall and sweeps in the outer layer was also observed in experiments (Grass, 1971; Krogstad *et al.*, 1992). For $y/\delta > 0.4$ K plays a stronger role than roughness.

Roughness induces mean-flow heterogeneity near the wall, as shown in Figure 9 by the contours of \tilde{U} and \tilde{V} (the difference between time-averaged velocity and time- and plane-averaged one) from Case K3R3 at $y = d$. The velocities are normalized by the value U at this elevation. Two main motions can be identified: the mean sweeping motion, highlighted by the correlation between long streaks of positive \tilde{U} and negative \tilde{V} , and the nearly vertical ejections, shown by locally high magnitudes of positive \tilde{V} . The

sweeping motions may correspond to the mean-flow “channeling phenomenon” observed on pyramid roughness by Hong *et al.* (2011). Such sweeps may be the upper part of the mean-flow re-circulation formed downstream of a relatively tall roughness element, similar to the case of a k -type bar roughness; the lower part of the recirculating flow, opposite to the direction of U_∞ , results in regions of positive f_d as the flow impinges on smaller roughness elements. Such mean flow heterogeneity is found mainly within the region $y < 2k$, to some degree coinciding with the roughness sub-layer thickness reported in the literature.

The mean-flow heterogeneity has a strong effect on coherent turbulent structures. In Figure 10 the contour lines of instantaneous negative u' are superposed on the \tilde{V} contours in the vertical plane and the \tilde{U} contours in the horizontal plane. The Figure shows the association of mean-flow ejections with the lift-up and breakup of low-speed

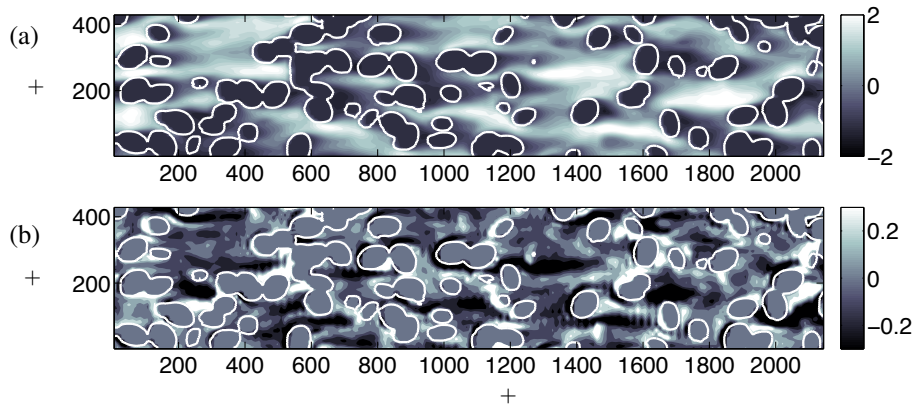


Figure 9. Contours of (a) \tilde{U} and (b) \tilde{V} at $y = d$ in case K3R3, normalized by U at this elevation. Contour lines show VOF value of 0.5 (i.e., borders of roughness elements).

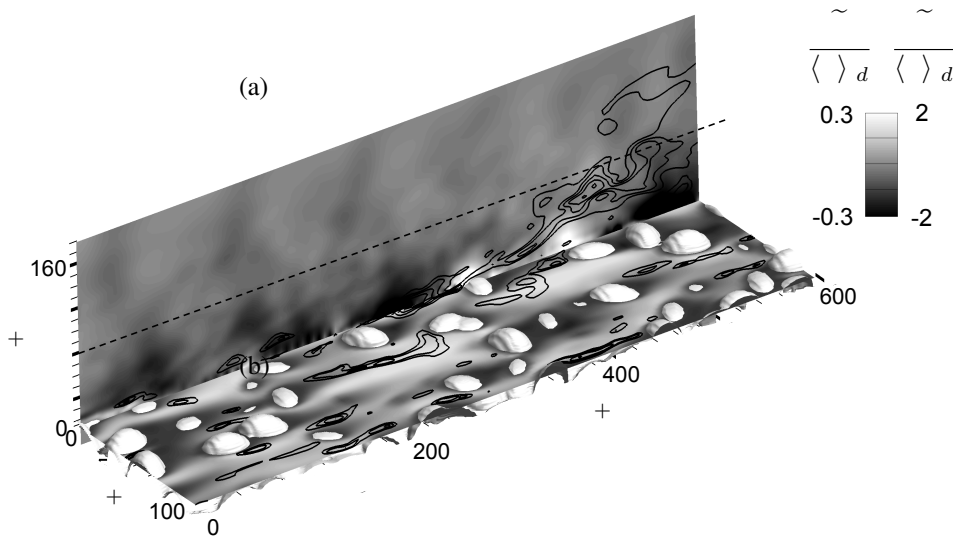


Figure 10. Contours of \tilde{U} (horizontal plane) at $y = d$, and \tilde{V} (vertical plane) with contour lines of instantaneous u' (contour levels from $-4.5u_\tau$ to $-1.5u_\tau$) in case K3R3; iso-surfaces show roughness elements.

streaks, and with turbulent production. As a result, the streaks on the plane $y = d$ become much shorter compared to the ones above a smooth wall, and are likely to terminate upstream of a relatively tall roughness element. The case with lower k^+ (e.g., case K3R1) does not produce the downward mean-flow streaks; instead, streaks are oriented mainly in the streamwise direction, except for weak vertical undulations, similar to structures on a d -type roughness. In this case, much weaker re-circulations are formed behind the the higher elements, and streaks are only weakly affected.

CONCLUSIONS

Large-eddy and direct numerical simulations are carried out for equilibrium sink flows over smooth and rough walls. Random, sand-grain-like roughness was used. The acceleration parameter, K , and the normalized roughness height, \bar{k} , are parameters quantifying, respectively, the acceleration and roughness effects. In the transitionally rough regime covered by the present simulations, the roughness Reynolds number $k^+ = \bar{k}u_\tau/\nu$ can be used as an indicator of the relative strength of these two effects.

Acceleration is found to decrease Re_θ and C_f , while

roughness increases both. When k^+ is kept constant, Re_θ and C_f are found to be dominantly affected by K and \bar{k} , respectively. Opposite effects of K and \bar{k} on the streamwise mean flow are also observed for current equilibrium FPG flows. A logarithmic region exist for most cases, and its slope is approximately the same as in zero-pressure-gradient boundary layers for all K and \bar{k} levels; only in a case in the reverse-transitional state the standard logarithmic layer is not observed. For the fully turbulent cases, the roughness function is found to depend on k^+ only, and agrees with experimental data obtained from non-accelerating flows with the same type of roughness.

Acceleration has the effect of decreasing the magnitude of the wall-normal Reynolds stress, while roughness increases both the streamwise and wall-normal components. The increase of $\langle v'v' \rangle$ in the lower part of the boundary layer with K observed by Cal *et al.* (2008) may be a phenomenon limited to the early stages of FPG flowsw. When the stresses are normalized by the friction velocity, wall similarity is found to apply to the fully turbulent cases only; in these cases, the effects of K and \bar{k} on $\langle u'u' \rangle$ and $\langle v'v' \rangle$ are comparable, and the wall-region profiles collapse for a constant k^+ .

Close to the wall ($y < 2k$), roughness generates mean-flow structures that take different patterns depending on the value of k^+ . The mean flow heterogeneity affects the lift-up and breakup of low-speed streaks.

ACKNOWLEDGMENTS

The authors acknowledge the financial support of the Natural Sciences and Engineering Research Council (NSERC) and Hydro Québec under the Collaborative Research and Development program. Computational support was supplied by the High Performance Computing Virtual Laboratory (HPCVL), Queen's University site. UP also acknowledges the support of the Canada Research Chairs Program. Professor Alberto Scotti kindly supplied the code to generate the sand grain roughness.

REFERENCES

- Cal, R.B., Brzek, B., Johansson, T.G. & Castillo, L. 2008 Influence of the external conditions on transitionally rough favorable pressure gradient turbulent boundary layers. *J. Turbul.* **9** (38), 1–22.
- Cal, R.B., Brzek, B., Johansson, T.G. & Castillo, L. 2009 The rough favourable pressure gradient turbulent boundary layer. *J. Fluid Mech.* **641**, 129–155.
- Chambers, F. W., Murphy, H. D. & McEligot, D. M. 1983 Laterally converging duct flows. Part 2. Temporal wall shear stress. *J. Fluid Mech.* **127** (403–428).
- Colebrook, C. F. 1939 Turbulent flow in pipes with particular reference to the transition region between smooth- and rough-pipe laws. *J. Inst. Civ. Eng.* **11**, 133–156.
- De Prisco, G., Keating, A. & Piomelli, U. 2007 Large-eddy simulation of accelerating boundary layers. *AIAA Paper 2007-0725*.
- Dixit, S. A. & Ramesh, O. N. 2008 Pressure-gradient-dependent logarithmic laws in sink flow turbulent boundary layers. *J. Fluid Mech.* **615** (1), 445–475.
- Dixit, S. A. & Ramesh, O. N. 2010 Large-scale structures in turbulent and reverse-transitional sink flow boundary layers. *J. Fluid Mech.* **649** (233–273).
- Esmaili, H. & Piomelli, U. 1993 Large-eddy simulation of relaminarizing sink flow boundary layers. In *Near-wall turbulent flows* (ed. R. M. C. So, C. G. Speziale & B. E. Launder), pp. 287–296. Amsterdam: Elsevier Science Publishers B. V.
- Finnigan, J. 2000 Turbulence in plant canopies. *Annu. Rev. Fluid Mech.* **32** (1), 519–571.
- Grass, A. J. 1971 Structural features of turbulent flow over smooth and rough boundaries. *J. Fluid Mech.* **50**, 233–255.
- Hong, J., Katz, J. & Schultz, M. P. 2011 Near-wall turbulence statistics and flow structures over three-dimensional roughness in a turbulent channel flow. *J. Fluid Mech.* **667**, 1–37.
- Jiménez, J. 2004 Turbulent flows over rough walls. *Annu. Rev. Fluid Mech.* **36**, 173–196.
- Jones, M. B., Marusic, I. & Perry, A. E. 2001 Evolution and structure of sink-flow turbulent boundary layers. *J. Fluid Mech.* **428**, 1–27.
- Jones, W. P. & Launder, B. E. 1972 Some properties of sink-flow turbulent boundary layers. *J. Fluid Mech.* **56** (02), 337–351.
- Keating, A., Piomelli, U., Bremhorst, K. & Nešić, S. 2004 Large-eddy simulation of heat transfer downstream of a backward-facing step. *J. Turbul.* **5** (20), 1–27.
- Kim, J., Moin, P. & Moser, R. D. 1987 Turbulence statistics in fully developed channel flow at low Reynolds number. *J. Fluid Mech.* **177**, 133–166.
- Krogstad, P.-Å., Antonia, R. A. & Browne, L. W. B. 1992 Comparison between rough- and smooth-wall turbulent boundary layers. *J. Fluid Mech.* **245**, 599–617.
- McEligot, D. M. & Eckelmann, H. 2006 Laterally converging duct flows. Part 3. Mean turbulence structure in the viscous layer. *J. Fluid Mech.* **549**, 233–273.
- Meneveau, C., Lund, T. S. & Cabot, W. H. 1996 A Lagrangian dynamic subgrid-scale model of turbulence. *J. Fluid Mech.* **319**, 353–385.
- Narasimha, R. 1985 The laminar-turbulent transition zone in the boundary layer. *Prog. Aerosp. Sci.* **22**, 29–80.
- Narasimha, R. & Sreenivasan, K. R. 1973 Relaminarization in highly accelerated turbulent boundary layers. *J. Fluid Mech.* **61**, 417–447.
- Narasimha, R. & Sreenivasan, K. R. 1979 Relaminarization of fluid flows. In *Adv. Applied Mech.*, vol. 19, pp. 221–309. New York: Academic Press Professional, Inc.
- Nikuradse, J. 1933 Strömungsgesetze in rauhen rohren. *VDI-Forsch.*
- Piomelli, U., Balaras, E. & Pascarelli, A. 2000 Turbulent structures in accelerating boundary layers. *J. Turbul.* **1** (1), 1–16.
- Raupach, M. R., Antonia, R. A. & Rajagopalan, S. 1991 Rough-wall boundary layers. *App. Mech Rev.* **44** (1), 1–25.
- Raupach, M. R. & Thom, A. S. 1981 Turbulence in and above plant canopies. *Annu. Rev. Fluid Mech.* **13**, 97–129.
- Scotti, A. 2006 Direct numerical simulation of turbulent channel flows with boundary roughened with virtual sandpaper. *Phys. Fluids* **18**, 031701.
- Spalart, P.R. 1986 Numerical study of sink-flow boundary layers. *J. Fluid Mech.* **172**, 307–328.
- Tachie, M. F., Agelinchaab, M. & Shah, M. K. 2007 Turbulent flow over transverse ribs in open channel with converging side walls. *Int. J. Heat Fluid Flow* **28** (683–707).
- Yuan, J. 2011 Large-eddy simulations of accelerating boundary-layer flows over rough surfaces. Master's thesis, Queen's University.